



**HAL**  
open science

# Investigation of rotor-stator interactions and laminar-turbulent transition using unsteady simulations and the Menter-Langtry model

Julien Marty, Benjamin François, Cédric Content

► **To cite this version:**

Julien Marty, Benjamin François, Cédric Content. Investigation of rotor-stator interactions and laminar-turbulent transition using unsteady simulations and the Menter-Langtry model. ETC 15 - European Turbomachinery Conference, Apr 2023, Budapest, Hungary. hal-04099284

**HAL Id: hal-04099284**

**<https://hal.science/hal-04099284>**

Submitted on 16 May 2023

**HAL** is a multi-disciplinary open access archive for the deposit and dissemination of scientific research documents, whether they are published or not. The documents may come from teaching and research institutions in France or abroad, or from public or private research centers.

L'archive ouverte pluridisciplinaire **HAL**, est destinée au dépôt et à la diffusion de documents scientifiques de niveau recherche, publiés ou non, émanant des établissements d'enseignement et de recherche français ou étrangers, des laboratoires publics ou privés.

# INVESTIGATION OF ROTOR-STATOR INTERACTIONS AND LAMINAR-TURBULENT TRANSITION USING UNSTEADY SIMULATIONS AND THE MENTER-LANGTRY MODEL

*Julien Marty<sup>1</sup> - Benjamin François<sup>1</sup> - Cédric Content<sup>2</sup>*

<sup>1</sup>DAAA, ONERA, Université Paris-Saclay, F-92190 Meudon - France

<sup>2</sup>DAAA, ONERA, Université Paris-Saclay, F-92320 Chatillon - France

## ABSTRACT

A significant part of the flow at the turbine blade walls can be laminar which influences the heat transfer and separation. Thus, the assumption of fully turbulent flow is not well suited for turbine applications. The present study aims at validating the Menter-Langtry transition model for unsteady flows. The configuration supporting this study is the CT3 turbine stage (TATEF2 project), experimentally tested at the van Karman Institute. To carry out unsteady simulations without simulating the full annulus configuration, a sliding interface technique is used, this latter handling no-match connectivities and relative motion between rotor and stator, and based on a reduced blade count leading to a contraction or a dilatation of the rotor-stator interface (the blade geometry is not modified). Thus, the model validation is completed by a comparison of this method with a steady-state simulation applying the mixing plane approach, classically used in turbine design. Moreover, as the *elsA* software enables the use of structured and unstructured meshes in the same computational domain, this validation is performed on both mesh types and some numerical guidelines are given to a relevant comparison between structured and unstructured meshes. The comparison to experimental data highlights a good agreement and validates the model to predict the time-averaged performances. For this configuration, only the unsteady simulations with a transition model are able to capture both isentropic Mach and Nusselt numbers over rotor and stator walls. Other simulations (steady one with or without transition model, unsteady one with a full turbulent flow assumption) fail at matching measurements. The mesh type and numerical approach effects are also reported.

## KEYWORDS

LAMINAR-TURBULENT TRANSITION, TURBINE, ROTOR-STATOR INTERACTION

## NOMENCLATURE

BFL	Blade Passing Frequency
FT	Fully turbulent results
$H_i$	Shape factor: $H_i = \frac{\delta_1}{\theta}$
HPT	High-Pressure Turbine
$M_{is}$	Isentropic Mach number
ML	Menter-Langtry results
$Nu$	Nusselt number
RoeV	Roe scheme with Venkatakrishnan limiter
S	Structured mesh
SST	Shear Stress Transport (turbulence model of Menter)
TKE	Turbulent Kinetic Energy
U	Unstructured mesh
$V_x$	Axial velocity component
$ W $	Magnitude of relative velocity
$\delta_1$	Displacement thickness of boundary layer
$\theta$	Momentum thickness of boundary layer

## INTRODUCTION

In order to reduce weight of turbofan engines, manufacturers aim at increasing stage loading of compressors and turbines. This can be achieved by using trans- or supersonic stages. Consequently, the flow topology is more complex than within a subsonic one. As mentioned by Sandberg and Michelassi [2022], sub- and supersonic stages, in opposition to isolated airfoils, are characterized by strong interactions between adjacent blades, allowing the significant deviation achieved in turbines, and between neighboring rows such as potential effects due to the small inter-row distance, incoming wakes influencing the flow inlet angle of downstream row. Moreover, the turbulence contained in wakes impacts the boundary layer evolution over blades of downstream rows. In supersonic configurations, the evolution of the pressure gradient is responsible for the generation of shock within the blade passage or at trailing edge. This leads to additional interactions: wake-shock, vortex-shock, causing higher losses. These features are commonly encountered in High-Pressure Turbine (HPT) where shocks are generated at the trailing edges of turbine vanes [Sieverding and Manna, 2020] and are responsible for huge fluctuations of stagnation pressure over the rotor, up to 40% [Dénos et al., 2000].

Thus, the life-cycle prediction of HPT depends on the prediction of the flow around blades, especially on the boundary layer development, in the framework of row interactions. Laminarity is important in HPT design for several reasons. Firstly, the heat transfer from the flow to the turbine blade depends strongly on the laminar-turbulent nature of the boundary layer. This quantity cannot be predicted accurately with an assumption of full-turbulent boundary layer. Secondly, turbine blades are high cambered and the flow is likely to separate. Boundary layer separation is also strongly dependent on the laminar-turbulent nature of the flow. Thirdly, in the inter-blade channels, the flow is accelerated and the flow may shift from a turbulent to a laminar state (relaminarization) with the associated impacts on the heat transfer and performance. For these reasons, the modeling of the laminar-turbulent transition in turbine design receives a growing attention. Consequently, many studies concentrated on HPT vane, such as the LS89 airfoil, experimentally tested at VKI [Arts and Lambert de Rouvroit, 1992] at different oper-

ating conditions and freestream turbulence intensities. By-pass transition [Garai et al., 2017, Cação Ferreira et al., 2019], shock-induced transition [Dupuy et al., 2020] can occur in this configuration.

Under unsteady conditions, encountered in stage configuration due to rotor-stator interaction, the transition mechanism can be strongly modified. When the wake generated by the previous blade impinges the airfoil, thanks to the boundary layer receptivity, the transition can be by-passed and the transition onset moves upstream. After the wake passage, the boundary layer is not strictly laminar but perturbations are observed within the boundary layer. The shape factor  $H_i$ , which is the ratio between displacement thickness and momentum thickness, decreases – and is below 2.59 – and the boundary layer is more able to overcome a strong adverse pressure gradient than a laminar one. Once the wakes are far from the airfoil and the perturbations are damped, the initial transition process can be newly observed up to the next wake passage. Similarly, shocks incoming from blades of the previous row impinge periodically blades, causing an unsteady shock-boundary layer interaction influencing the laminar-turbulent transition process.

In order to better understand the flow physics within a HPT, several laboratories work on a turbine stage. Guenette et al. [1989] investigated heat transfer of a transonic turbine stage and proved similarity of flow at midspan, with 2-D cascade with passing bars. Gaetani et al. [2006] studied the rotor-stator interaction of a turbine stage through five-hole probe and a temperature gauge, highlighting the evolution of the flow across the stage, the modification of secondary flows. The work of Paniagua et al. [2008] focused on unsteady interaction between vane shocks and rotor blades. The shock impingement is responsible for a small separation over the rotor blade, close to the leading edge, which periodically moves. The present work is based on the computations performed in Paniagua et al. [2008] with *elsA* software. The transition model of Arnal et al. [1984] was applied on the stator blade, only. However, this model is dedicated to natural transition (freestream turbulence intensity lower than 1%) in which the transition onset is due to the instability of Tollmien-Schlichting waves. Conversely, HPT is characterized by high freestream turbulence, by by-pass or shock-induced transition. Thus, the present study aims at improving the flow prediction by using a more adapted transition model. On CFD side, other authors investigate the unsteady flow in turbine stage using transition model, as the Laminar Kinetic Energy model [Pacciani et al., 2012], or not [Tallman et al., 2009, Pinelli et al., 2021]. Nonetheless, the unsteady transition is mainly predicted using high-fidelity methods such as Large Eddy Simulation [Papadogiannis et al., 2016, Leggett et al., 2022].

As earlier mentioned, the present work is based on CFD computations performed by Paniagua et al. [2008] and focuses on the evaluation of the Menter-Langtry [Menter et al., 2006, Langtry and Menter, 2009] transition model on a turbine stage with unsteady simulations techniques and on both structured and unstructured grids. Firstly, the turbine stage is presented, followed by the turbulence and transition modelings used as well as the numerical setup. Then, the validation of the model is carried out step by step, from steady to unsteady simulations, from structured to unstructured meshes.

## **STAGE-CONFIGURATION CT3**

### **Experimental facility**

The present study focuses on the experimental turbine stage CT3 used in TATEF2 project [Dénos et al., 2000, De la Loma et al., 2008, Paniagua et al., 2008]. This turbine stage is representative of modern high-pressure turbine. The experimental setup includes measurements on the blade walls for the pressure and the heat flux (see Fig. 1). Different aerodynamic loadings (pressure ratios between outlet and inlet) have been tested during the experimental campaign.

The highest aerodynamic loading ( $P_{\text{inlet}}/P_{\text{outlet}} = 5.12$ ) has been selected for the present study. The key parameters of the operating point are recalled in Table 1. It should be noticed that only the "High" condition is considered in this investigation. The freestream turbulence intensity at the turbine inlet was measured by hot-wires and is equal to 5% at midspan, as mentioned in Yasa et al. [2006]. In 3D case, close to endwalls, this value increases up to 25% or even 45%, as the velocity magnitude is very low.

Rotating speed	6474 rpm
Reynolds number	$1.1 * 10^6$
Outlet isentropic Mach number (plane 2)	1.249
Outlet isentropic Mach number (plane 3)	1.18
Blade wall temperature	288.5 K
Inlet stagnation pressure	1.65 bar
Inlet stagnation temperature	434 K
Inlet turbulence rate	5 %

Table 1: Operating conditions ("High" condition)

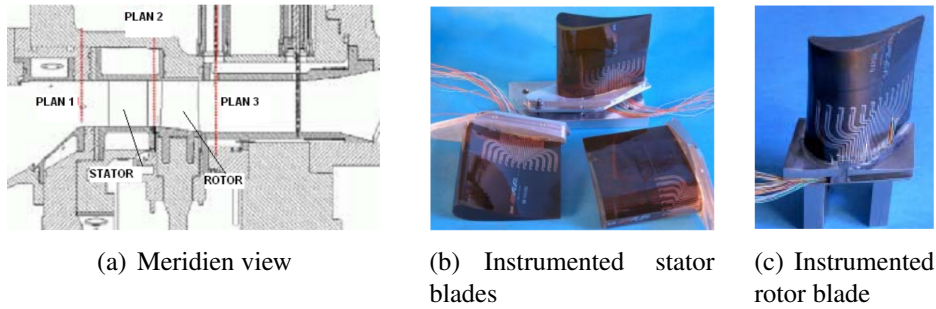


Figure 1: Experimental set-up - CT3 turbine

The main geometrical features of the turbine stage are recalled in the Table 2.

	Stator	Rotor
Blade number	43	64
Axial chord [mm]	41.16	39.78
Axial chord/span	0.812	0.738
Hub-to-tip ratio	0.872	0.864
Stagger angle [deg]	54	32

Table 2: Geometrical features at mid-span

### Numerical simulation setup

Figure 2 presents the mesh used for the 2.5D simulations, relative to the flow at midspan. This mesh is based on the work of Paniagua et al. [2008]. Thus, there is no grid dependence study in the present work. It should be noticed that upper and lower boundaries of this 2.5D configuration are based on information coming from the 3D one. The spanwise height represents

a little less than 1% of massflow. Only one single blade channel is shown here. 100 points are used in the streamwise direction between the leading-edge and the trailing-edge for both blades. In the inter-blade channels, 150 points and 160 points are used in the azimuthal direction for the stator and the rotor respectively.

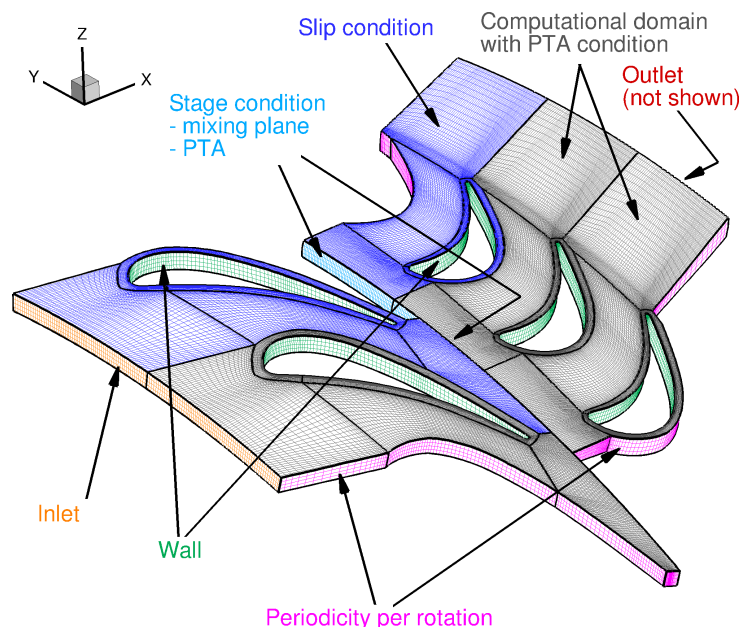


Figure 2: Mesh for 2.5D configuration

On the CT3 configuration, steady and unsteady RANS simulations were performed. To reduce the CPU cost of the simulation, RANS simulations are performed on a computational domain comprising only one blade passage per row while URANS simulations are based on a computational domain reduced to two stator channels and three rotor channels, allowing the use of the technique developed by Fourmaux [1994] for the unsteady simulation. This technique, also called Profile Transformation Approach (PTA), is close to the blade count reduction approach but the reduction is only applied at the rotor-stator interface (i.e. at the same location of the mixing plane). Thus, there is no rescale of geometry. With the present reduction, the azimuthal arc length is nearly the same between the two rows ( $16.74^\circ$  vs  $16.88^\circ$ ). For the present application, the assumption is acceptable. It must be kept in mind that this unsteady technique modify the Blade Passing Frequency (BPF), especially if the rotor and stator blade numbers are prime. The evaluation is made in Table 3. Differences are below 1% and therefore acceptable for the intended flow physics to capture.

Computations were undertaken with the compressible Navier-Stokes solver *elsA*, software developed by ONERA and co-owned by Safran and ONERA [Cambier et al., 2013], using the Roe approximate Riemann solver [Roe, 1981] with a second order MUSCL reconstruction smoothed by a Van Albada [van Albada et al., 1997] or a Venkatakrishnan limiter [Venkatakrishnan, 1995], and a scalar LUSSOR implicit method [Yoon and Kwak, 1991].

The steady computations rely on a first order in time backward Euler scheme while the URANS simulations are performed with a second order time scheme [Gear, 1971]. The number of sub-iterations is variable (a minimum of 5 is always performed), a convergence threshold at 0.01 is imposed at each timestep. Thus, this ensure a good accuracy of the transient flow

	Stator	Rotor
Azimuthal extent [°]	16.74	16.88
$BPF_{\text{real}}$ [ $\Omega$ ]	64	43
$BPF_{\text{current}}$ [ $\Omega$ ]	64.5	42.66
Ratio $BPF_{\text{current}}/BPF_{\text{real}}$	1.0078	0.9922
Number of timesteps per blade passage	644.96	426.64
Number of timesteps per revolution	27511.27	

Table 3: Timesteps and Blade Passing Frequencies (BPF) in the unsteady simulation based on the technique of Fourmaux [1994]

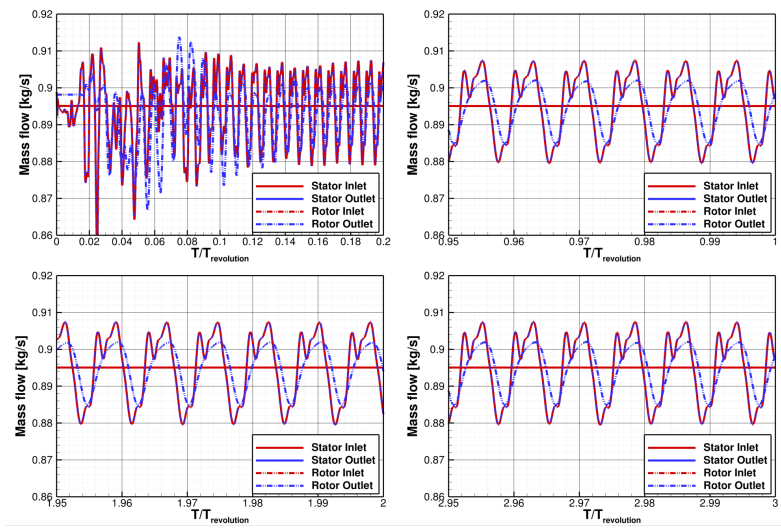


Figure 3: Mass flow time evolution

prediction. As indicated in Table 3, 27,511 timesteps are performed per complete revolution, namely around 430 for each rotor blade passage and 640 for each stator blade passage. For each simulation, three complete revolutions are performed, as shown in Figure 3, the first one being devoted to the transient part, and the last one to the time-average flow computation. The temporal evolution of mass flow at four stations (stator inlet, stator outlet, rotor inlet and rotor outlet) shows that the periodic convergence is reached after one revolution. Another revolution is computed in order to check the temporal periodicity accuracy, and finally the third revolution is used for the time-average computation and the post-processing. Periodic boundary conditions are used for the azimuthal boundary for both the steady and unsteady simulation. At the inlet, the subsonic boundary condition is used. Inlet stagnation pressure, temperature are imposed as well as an axial flow direction. The turbulence kinetic energy is deduced from the inlet turbulence rate. For the second turbulence variable  $\omega$ , a laminar-turbulent viscosity ratio of 35 is assumed (based on previous experiences with the simulation of the LS89-MUR241 [Benyahia, 2012]). The first transition variable  $\rho\gamma$  is set to 1 while the second  $\rho\overline{Re}_\theta$  to 122. At the outlet, the simplified radial equilibrium is imposed and based on the pressure ratio earlier defined. At the blade walls, a no-slip isotherm boundary condition is used. The imposed wall temperature is  $T_b = 288.5K$ . In this study, the wall is considered smooth i.e. without any roughness influencing the boundary layer development. There is no information on the wall surface condition

in experiments. The  $\Delta y^+$  value is lower than 0.75, except close to the leading edge where the maximum value is 1.5. As only 2.5D configurations are considered in the present study, slip boundary conditions are used for the lower and upper radius borders, as these boundaries represent streamlines in 3D configurations.

### **Turbulence and transition models**

In the present study, the laminar-turbulent transition is modeled through the Menter-Langtry model [Menter et al., 2006, Langtry and Menter, 2009], except that the correlations used are those of Content and Houdeville [2010]. These correlations, called CH10, were built from two experimental datasets (a flat plate and a ogive cylinder with various inlet turbulence rates and pressure gradients). The Menter-Langtry model is composed of two transport equations: one for the intermittency  $\gamma$  and one for the transition Reynolds number  $\overline{Re}_\theta$ . The intermittency variable  $\gamma$  denotes if the boundary layer is laminar ( $\gamma = 0$ ), fully turbulent ( $\gamma = 1$ ) or in a transient state ( $0 < \gamma < 1$ ). Outside the boundary layer, this value must be equal to 1.

This transition model is coupled with  $k - \omega$  Menter SST model [Menter, 1994]. Accounting for the transition model requires to modify some terms in the turbulence model, especially production and destruction terms which are multiplied by the effective intermittency defined by  $\gamma_{\text{eff}} = \max(\gamma, \gamma_{\text{sep}})$ . More informations about this model implemented in *elsA*, are given in Bouchard et al. [2021], Dufau et al. [2021].

## **RESULTS ON STRUCTURED GRIDS**

### **Flow analysis**

Figure 4 depicts the iso-contours of relative velocity magnitude  $|W|$  (left), axial velocity  $V_x$  (middle) and turbulent kinetic energy TKE (right) at three different instants:  $t = nT$ ,  $nT + \frac{T}{4}$  and  $nT + \frac{3T}{4}$  where  $T$  is the rotor period and,  $n$  the rotation number (2, in the present case). Those variables highlight the features of the flow around blades, such as acceleration or deceleration, separations, wakes, shock as well as interactions between them. Besides, the comparison between the three instants allow following the temporal evolution of identified features. It should be noted that the inlet Mach number is 0.15. Thus, flow is strongly accelerated in the stator passage due to the favorable pressure gradient and the convergent interblade channel. This becomes supersonic at the channel outlet, generating two oblique shock waves at the trailing edge. Downstream, the flow remains mainly supersonic. The first shock, (a) on figure 4(b), impacts the adjacent blade, creating a separation bubble responsible for the laminar-turbulent transition, as shown later thanks to the Nusselt number distribution over blade walls. The second shock (b) is oriented towards the rotor. With a steady-state simulation based on mixing plane approach, the interaction between this shock and the rotor is not accounted for. On the contrary, this stator-rotor interaction is responsible for the creation and disappearing of a small separation bubble - in which the laminar-turbulent transition occurs - over the rotor suction side, close to the leading edge, during a stator passage. According to the location of the rotor blade relative to the second shock (b), the flow at the leading edge differs significantly. When the shock impinges the rotor blade, (f) on figure 4(e), the boundary layer separates, causing the forming of a separation bubble in which transition occurs. On the contrary, when the shock is far from the blade, a separation bubble appears more downstream (g), close the axial position at 70 mm. For some specific instant, the separation bubble is not observed at the maximum thickness of the rotor blade (e). This can result from the interaction between the wake (c) and the second shock of the adjacent stator blade, which are responsible for a very small bubble at the leading edge, as shown by TKE contours.

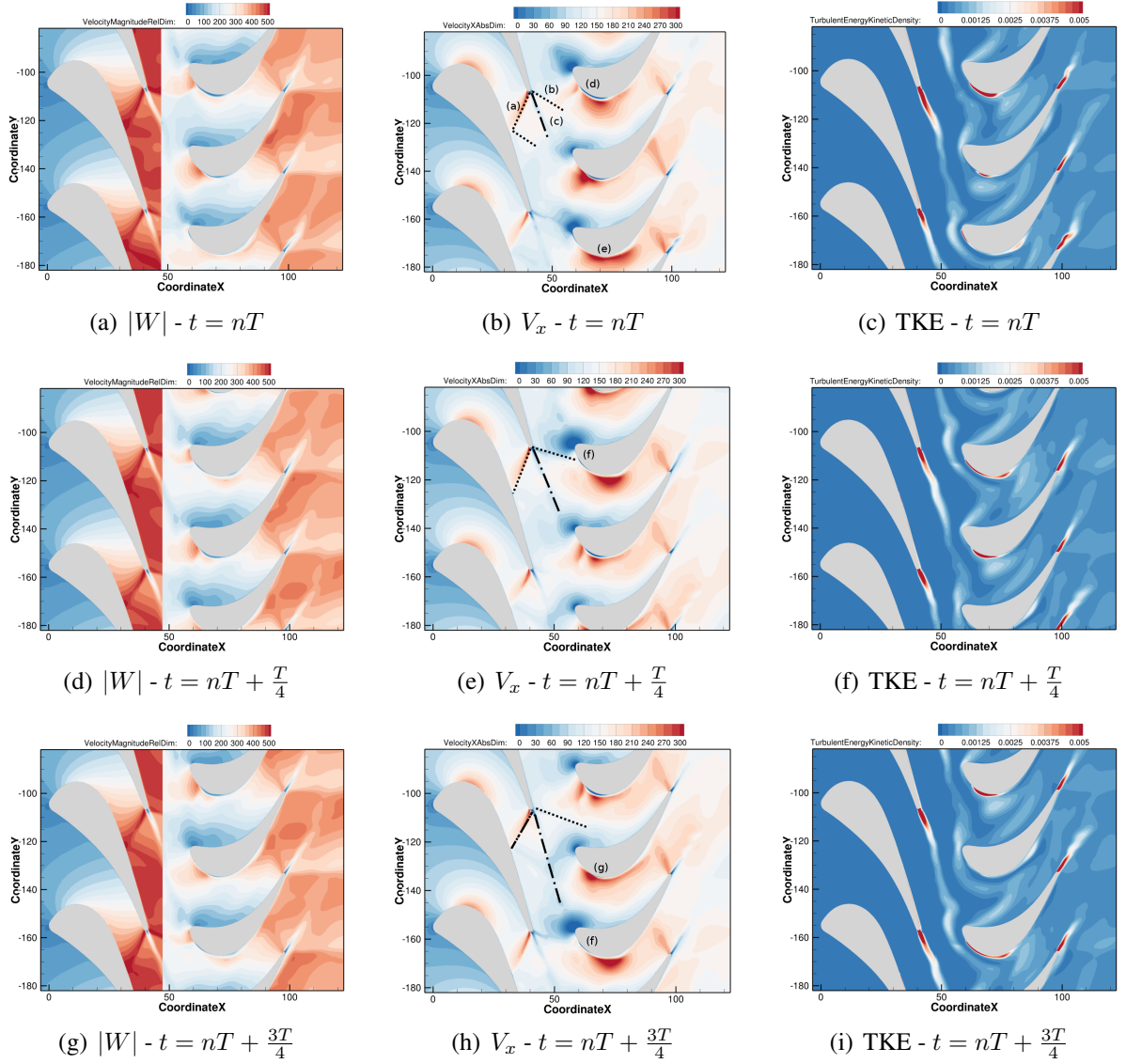


Figure 4: Contours of relative velocity magnitude  $|W|$  (left), axial velocity  $V_x$  (middle) and turbulent kinetic energy TKE (right) at three different instants showing the flow complexity at midspan

Because the relative velocity is very tangential downstream the stator, the inlet relative Mach number in the rotor domain is subsonic. The flow accelerates before the entrance of the inter-blade channel because of the high camber of the suction side of the rotor, as shown by the magnitude of relative velocity. A supersonic area is visible on the suction side of the rotor, close to the leading-edge. The inter-blade passage between rotors forms a converging duct. The same phenomenon arises in the rotor: the flow becomes supersonic at the outlet of the channel, leading to the appearance of two shock waves at the rotor trailing edge, similarly to the stator. On pressure side, the shock is oriented towards the adjacent blade. This shock is strongly attenuated due to expansion. Nonetheless, the impact on suction side, close to three quarters of chord, is responsible for a low velocity region. This feature depends also on the state of the upstream boundary layer. For example, at  $t = nT + \frac{3T}{4}$ , the boundary layer over the middle

rotor blade is not fully turbulent as the turbulent kinetic energy is quite small. Consequently, the shock-boundary layer interaction results in a thickening of the boundary layer.

Thus, the flow complexity can be summarized by: (i) the laminar-turbulent transition is induced by a shock over stator suction side and by an unsteady separation bubble resulting from a shock - boundary layer interaction over the rotor suction side and (ii) a boundary layer separation occurs in the vicinity of the rotor trailing edge, over the suction side. The prediction of all these phenomena is strongly influenced by the flow modeling and the numerical setup.

### Steady computations

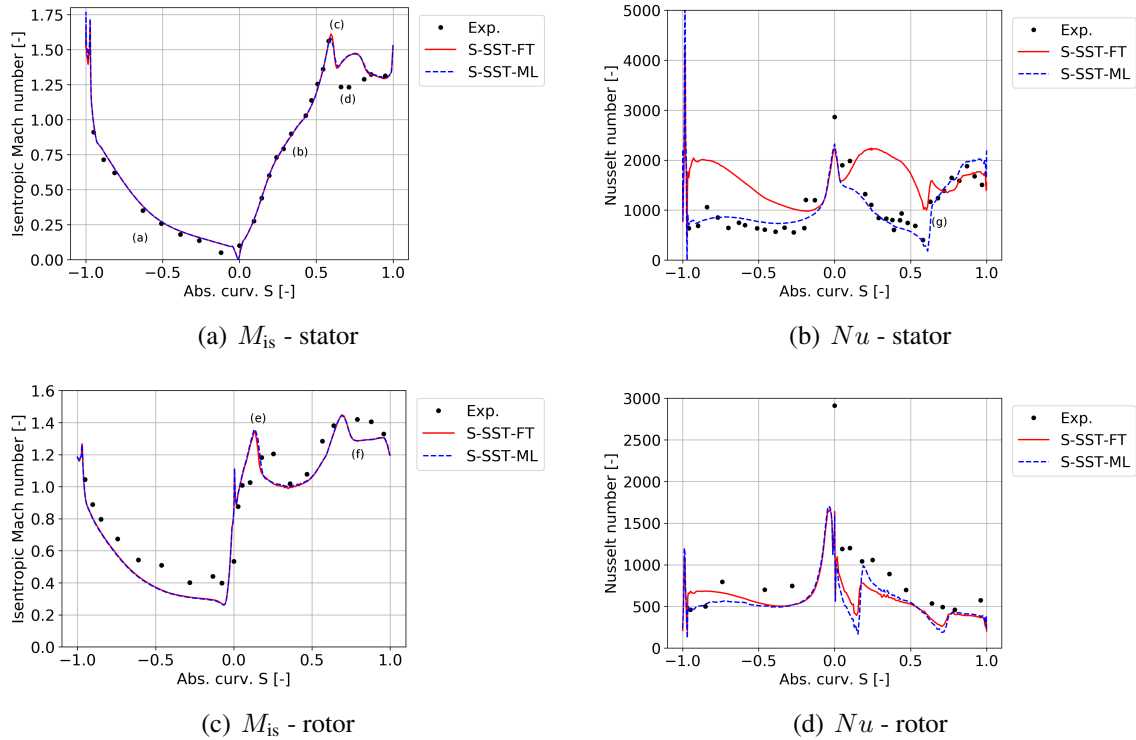


Figure 5: Distribution of isentropic Mach (left,  $M_{is}$ ) and Nusselt (right,  $Nu$ ) numbers over stator (top) and rotor (bottom) blades predicted by steady computation on structured grids with fully turbulent assumption and transition modeling

Figure 5 shows the distribution of static pressure and heat flux in terms of isentropic Mach and Nusselt numbers over the stator and the rotor blades, along with the curvilinear abscissa. Negative and positive values of abscissa are relative to the pressure ((a) on the figure) and the suction side (b), respectively. Numerical results are obtained by assuming the flow as fully turbulent (FT) or by modeling the laminar-turbulent transition (ML) and only the structured mesh is used in this subsection. The effect of transition model is quite small on the isentropic Mach number distribution. Both simulations show a peak over the suction side of the stator (c) which is the footprint of the impact of the shock wave generated by the trailing edge of adjacent stator blade. Numerical data agree well with experiments, except downstream of the shock (d). The separation bubble induced by the shock is not well predicted. Similarly, over the rotor blade, the main discrepancy with the experiments are obtained downstream of the shock generated at the rotor trailing edge (f), not by the stator trailing edge (e).

The transition modeling is of primary importance in order to well predict the Nusselt number. With a fully turbulent flow (S-SST-FT), heat fluxes are over-predicted, all along the stator blade, except over the suction side near the trailing edge as the laminar-turbulent transition has occurred due to the shock impact (g). Over the rotor blade, both simulations clearly fail to predict the Nusselt number distribution. The main hypothesis is the lack of rotor-stator interaction as the mixing plane acts as an azimuthal average and remove wake and interaction of the shock wave generated at stator trailing edge with the rotor boundary layer. In the following, only numerical results accounting for transition are considered.

### Unsteady computations

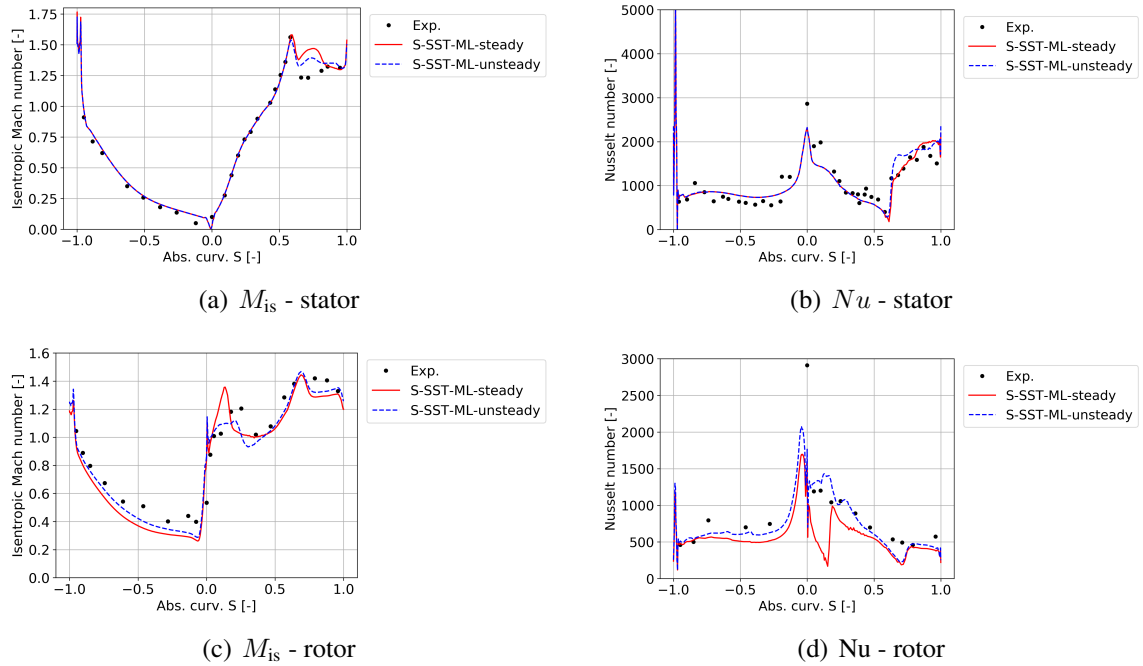


Figure 6: Distribution of isentropic Mach (left,  $M_{is}$ ) and Nusselt (right,  $Nu$ ) numbers over stator (top) and rotor (bottom) blades predicted by steady and unsteady computations on structured grids with transition modeling

The isentropic Mach number and Nusselt number are plotted in Figure 6. On the stator blade, the unsteady effects are only observed over the suction side and close to the trailing edge. This is expected as the flow is choked in the stator: the interaction with the rotor blade leads to small fluctuations which do not cross the throat of the stator inter-blade channel. The comparison between steady and time-averaged unsteady data shows that the static pressure plateau downstream the boundary layer - shock interaction is strongly influenced by rotor-stator interaction and a better prediction is obtained. Even if differences still remain on the rotor blade, the agreement with experimental data is improved thanks to the unsteady simulation. This means that the stator influences also the pressure distribution within separation over rotor blade wall. On the pressure side, the agreement is better with unsteady simulation.

Concerning the heat flux and the predicted Nusselt number, the distribution is quite similar over suction side between steady and unsteady simulations, except downstream of the shock where the steady computation is oddly in better agreement with experiments. Over the rotor

wall, the predicted is significantly better when stator-rotor interactions are taken into account in the simulation. The Nusselt profile over the suction side is recovered with the unsteady simulation.

Thus, at least for this test case, stator-rotor interaction and transition modeling must be accounting for in order to well predict the Nusselt distribution over both stator and rotor walls.

## RESULTS ON UNSTRUCTURED GRIDS

As the *elsA* software handles both structured and unstructured meshes, the transition model was also implemented for unstructured grids. The present investigation focuses on the validation of this implementation, not on the best practice in terms of creating an optimal unstructured mesh (prism layer or not, thickness of this layer, aspect ratio for tetrahedrons, ...). Thus, it was decided to use only hexahedrons in order to be fully comparable to structured mesh. However, the numerical setup cannot be strictly identical between these two mesh topologies. Before validating the transition model, the effect of numerical parameters must be investigated. In the present study, the choice was made to keep the Roe scheme. Thus, the focus concerns the MUSCL limiter.

### Influence of numerical setup

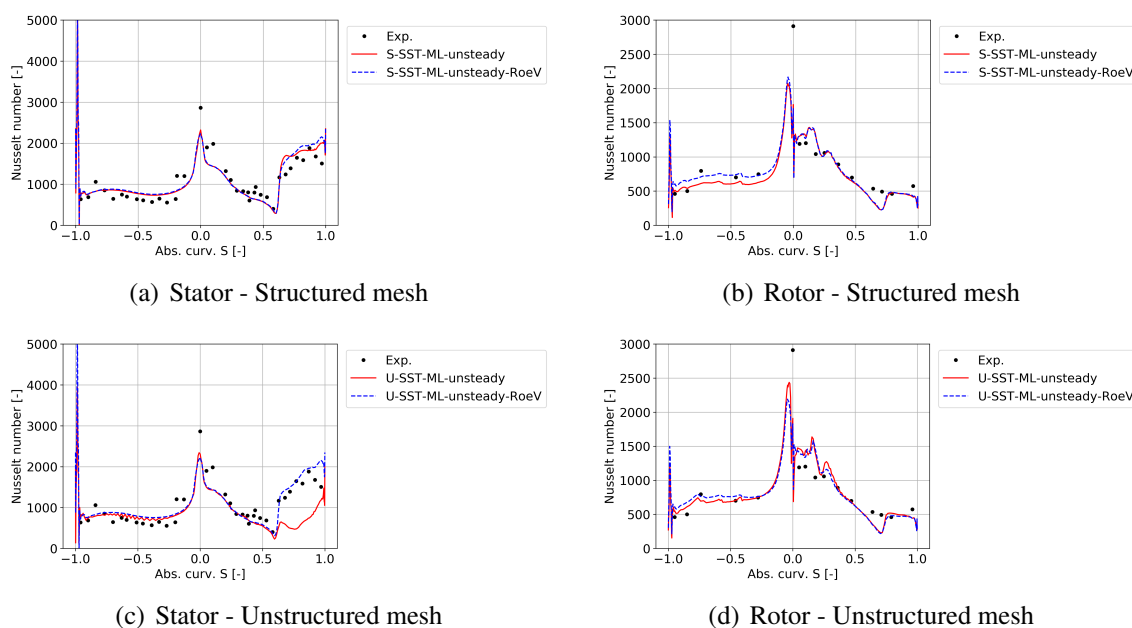


Figure 7: Nusselt number distribution over stator (left) and rotor (right) blades predicted by unsteady simulations accounting for laminar-turbulent transition, on structured (top) and unstructured (bottom) meshes

As discrepancies appear mainly on the Nusselt number, the following analysis relies only on this quantity. With the structured grid, the limiter linked to the Roe scheme, influences mainly the Nusselt distribution, over the suction side, close to the trailing edge, i.e. downstream of the shock. The limiter of Venkatakrisnan allows a better prediction of the heat flux rise. However, the agreement with experimental data is quite similar. On the rotor, there is no significant effect on the suction side while a better agreement is reached on the pressure side. In the present

study, the unstructured mesh is a fully hexaedric one, comprising the same cell number. In other words, the mesh is identical and only the way to describe the mesh differs. The comparison of the Nusselt distribution over the suction side shows that the van Albada limiter behaves wrong downstream of the shock, leading to a mis-prediction of the heat flux rise due to the laminar-turbulent transition. Moreover, some oscillations are observed on the pressure side. On the rotor, the discrepancies are much more smaller, leading to a similar agreement with experimental data. As shown by the work by Jawahar and Kamath [2000], the limiter of Venkatakrishnan is better than the one of van Albada, as this is a multidimensional limiter, which improves the robustness and accuracy by yielding oscillation-free solutions and recovering the second order of the numerical scheme. On the contrary, the van Albada limiter is not sufficiently effective in removing oscillations at discontinuities with unstructured meshes. In *elsA* software, this has been proved on several test cases during the PhD of Soismier [2016]. In the following, only the Venkatakrishnan limiter is used, for both structured and unstructured grids in order to validate the implementation of the transition model for unstructured mesh.

## Validation

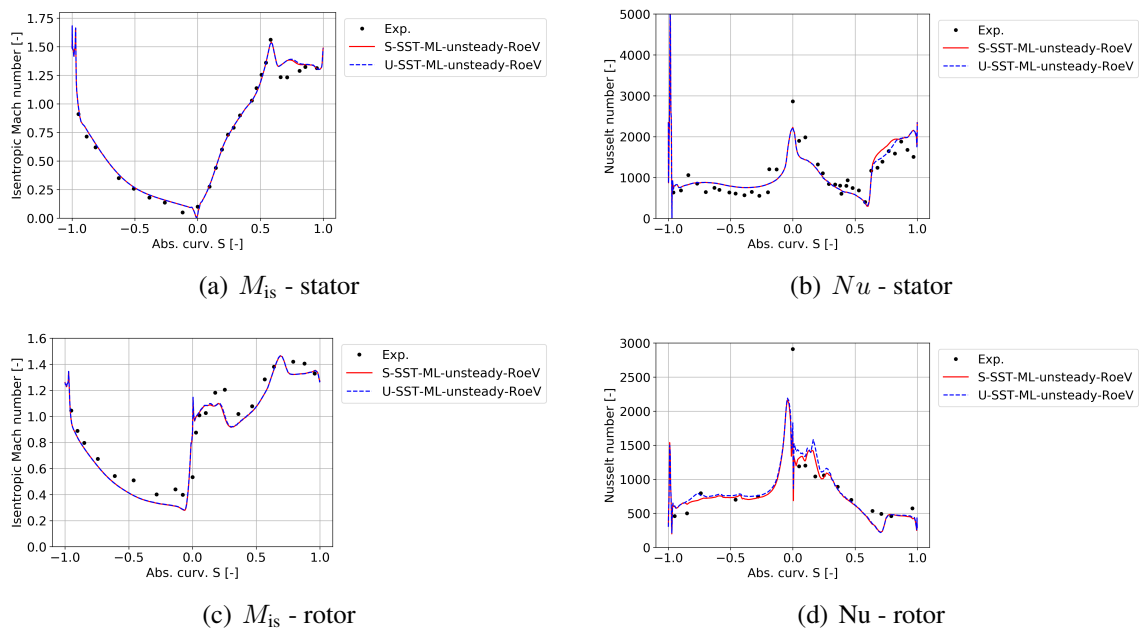


Figure 8: Distribution of isentropic Mach (left,  $M_{is}$ ) and Nusselt (right,  $Nu$ ) numbers over stator (top) and rotor (bottom) blades predicted by unsteady computations on structured and unstructured grids with transition modeling and the Venkatakrishnan limiter

The isentropic Mach number and the Nusselt number distributions over stator and rotor walls are plotted in Figure 8, for the two mesh types considered in this study. It should be noticed that the post-processing is identical for both structured and unstructured meshes. The isentropic Mach number curves are very close together as only a very small discrepancy is observed downstream of the shock impact. Concerning the Nusselt number, the agreement between numerical results is good over the stator wall as the main difference appears in the downstream part of the suction side and reveals that the production of turbulence is not strictly identical leading to a small mismatch in terms of heat flux. Over the rotor blade, the agreement

is less satisfactory due to the difference in terms of upstream turbulence coming from the stator and of turbulence production. Nonetheless, the agreement with experiments is still good. Thus, the transition model of Menter-Langtry is validated for both grid types.

## CONCLUSIONS

The present investigation is dedicated to the impact of rotor-stator interaction on laminar-turbulent transition over turbine airfoils. The aim of this study is the validation of the Menter-Langtry transition model implemented in the *elsA* software to predict the unsteady flow and time-averaged performances of the CT3 stage configuration (TATEF2 project), on both structured and unstructured meshes. As a reminder this study aims at improving the flow modeling used by Paniagua et al. [2008], to the Menter-Langtry model. However, this must be continued by applying this model on the 3D mesh for a more rigorous validation.

The analysis of the time-averaged performances underlined that transition modeling and unsteady modeling were both necessary to get consistent results with the measurements (isentropic Mach number and Nusselt number distributions on the blade) for the CT3 turbine. Numerical parameters can have a strong influence on CFD results, especially if their behavior differs from structured to unstructured grids. In the present study, with the Roe scheme, the main parameter is the limiter. On unstructured grid, the Venkatakrishnan limiter is used to recover consistent results with structured grids, allowing the validation of the Menter-Langtry transition model.

Further works are driven by three objectives: validation of the model on 3D configuration with unsteady effects, a better comprehension of physical mechanisms involved in transition trigger (role of shock, of wake...) thanks to high fidelity simulations (e.g. wall-resolved large eddy simulation).

## ACKNOWLEDGEMENTS

All simulations have been performed in the framework of the *elsA* agreement between SAFRAN and ONERA, which are co-owners of this software. This work was partially supported by the SONICE project, granted by the French Directorate General for Civil Aviation (DGAC).

## REFERENCES

- D. Arnal, M. Habiballah, and E. Coustols. Théorie de l'instabilité laminaire et critères de transition en écoulement bi et tridimensionnel. *La Recherche Aérospatiale*, 2:125–143, Mars-Avril 1984.
- T. Arts and M. Lambert de Rouvroit. Aero-Thermal Performance of a Two-Dimensional Highly Loaded Transonic Turbine Nozzle Guide Vane: A Test Case for Inviscid and Viscous Flow Computations. *Journal of Turbomachinery*, 114(1):147–154, 01 1992. ISSN 0889-504X. doi: 10.1115/1.2927978. URL <https://doi.org/10.1115/1.2927978>.
- A. Benyahia. *Mise en oeuvre et évaluation d'un modèle de transition à équations de transport pour la simulation d'écoulements en turbomachines*. PhD thesis, ISAE, 2012.
- M. Bouchard, J. Marty, S. Deck, and M. Costes. Validation of correlations-based transition modeling strategies applied to the spalart-allmaras turbulence model for the computation of separation-induced transition. *Aerospace Science and Technology*, 119:107045, 2021. ISSN 1270-9638. doi: <https://doi.org/10.1016/j.ast.2021.107045>. URL <https://www.sciencedirect.com/science/article/pii/S1270963821005551>.
- T. S. Cação Ferreira, N. Vasilakopoulos, and T. Arts. Investigation of Thermal Effect on Bypass Transition on a High-Pressure Turbine Guide Vane. *Journal of Turbomachinery*, 141(5), 01 2019. ISSN 0889-504X. doi: 10.1115/1.4041909. URL <https://doi.org/10.1115/1.4041909>. 051006.

- L. Cambier, S. Heib, and S. Plot. The Onera elsA CFD Software: Input from Research and Feedback from Industry. *Mechanics & Industry*, 14:159–174, 1 2013. ISSN 2257-7750. doi: 10.1051/meca/2013056. URL [http://www.mechanics-industry.org/article\\_S2257777713000560](http://www.mechanics-industry.org/article_S2257777713000560).
- C. Content and R. Houdeville. Local correlation-based transition model. In *8th International ERCOFTAC Symposium on Engineering Turbulence Modelling and Measurements*, pages 522–527, June 9-11 2010.
- A De la Loma, G Paniagua, D Verrastro, and P Adami. Transonic turbine stage heat transfer investigation in presence of strong shocks. *Journal of Turbomachinery*, 130(3):031019, 2008.
- R. Dénos, T. Arts, G. Paniagua, V. Michelassi, and F. Martelli. Investigation of the Unsteady Rotor Aerodynamics in a Transonic Turbine Stage. *Journal of Turbomachinery*, 123(1):81–89, 02 2000. ISSN 0889-504X. doi: 10.1115/1.1314607. URL <https://doi.org/10.1115/1.1314607>.
- A. Dufau, J. Marty, D. Man, and E. Piot. Simulation of Passing Wakes Inducing Unsteady Boundary Layer Transition Around Low-Pressure Turbine Blade. volume Volume 2B: Turbomachinery "Axial Flow Turbine Aerodynamics; Deposition, Erosion, Fouling, and Icing" of *Turbo Expo: Power for Land, Sea, and Air*, 06 2021. doi: 10.1115/GT2021-58563. URL <https://doi.org/10.1115/GT2021-58563>. V02BT32A001.
- D. Dupuy, L. Gicquel, N. Odier, F. Duchaine, and T. Arts. Analysis of the effect of intermittency in a high-pressure turbine blade. *Physics of Fluids*, 32(9):095101, 2020. doi: 10.1063/5.0018679. URL <https://doi.org/10.1063/5.0018679>.
- A. Fourmaux. Assessment of a low storage technique for a multi-stage turbomachinery Navier-Stokes computations. Rapport Technique TP 1994-157, ONERA, 1994.
- P. Gaetani, G. Persico, V. Dossena, and C. Osnaghi. Investigation of the Flow Field in a High-Pressure Turbine Stage for Two Stator-Rotor Axial Gap - Part I: Three-Dimensional Time-Averaged Flow Field. *Journal of Turbomachinery*, 129(3):572–579, 07 2006. ISSN 0889-504X. doi: 10.1115/1.2472383. URL <https://doi.org/10.1115/1.2472383>.
- A. Garai, L. T. Diosady, S. M. Murman, and N. K. Madavan. Scale-Resolving Simulations of Bypass Transition in a High-Pressure Turbine Cascade Using a Spectral Element Discontinuous Galerkin Method. *Journal of Turbomachinery*, 140(3), 12 2017. ISSN 0889-504X. doi: 10.1115/1.4038403. URL <https://doi.org/10.1115/1.4038403>. 031004.
- C. William Gear. *Numerical Initial Value Problems in Ordinary Differential Equations*. Prentice Hall PTR, USA, 1971. ISBN 0136266061.
- G. R. Guenette, A. H. Epstein, M. B. Giles, R. Haimes, and R. J. G. Norton. Fully Scaled Transonic Turbine Rotor Heat Transfer Measurements. *Journal of Turbomachinery*, 111(1):1–7, 01 1989. ISSN 0889-504X. doi: 10.1115/1.3262231. URL <https://doi.org/10.1115/1.3262231>.
- P. Jawahar and H. Kamath. A high-resolution procedure for euler and navier-stokes computations on unstructured grids. *Journal of Computational Physics*, 164(1):165–203, 2000. ISSN 0021-9991. doi: <https://doi.org/10.1006/jcph.2000.6596>. URL <https://www.sciencedirect.com/science/article/pii/S0021999100965963>.
- R.B. Langtry and F.R. Menter. Correlation-Based Transition Modeling for Unstructured Parallelized Computational Fluid Dynamics Codes. *AIAA Journal*, 47(12):2894–2906, 2009. doi: 10.2514/1.42362.
- J. Leggett, Y. Zhao, and R. D. Sandberg. High-Fidelity Simulation Study of the Unsteady Flow Effects on High-Pressure Turbine Blade Performance. *Journal of Turbomachinery*, 145(1), 10 2022. ISSN 0889-504X. doi: 10.1115/1.4055576. URL <https://doi.org/10.1115/1.4055576>. 011002.
- F.R. Menter. Two-equation eddy-viscosity turbulence models for engineering applications. *AIAA Journal*, 32(8): 1598–1605, August 1994.

- F.R. Menter, R.B. Langtry, S.R. Likki, Y.B. Suzen, P.G. Huang, and S. Völker. A Correlation-Based Transition Model Using Local Variables Part I - Model Formulation. *Journal of Turbomachinery*, 128:413–422, July 2006. doi: 10.1115/1.2184352.
- R. Pacciani, M. Marconcini, A. Arnone, and F. Bertini. Urans analysis of wake-induced effects in high-lift low reynolds number cascade flows. In *ASME Turbo Expo, June 11-15, Copenhagen, Denmark, GT2012-69479*, 2012.
- G. Paniagua, T. Yasa, A. de la Loma, L. Castillon, and T. Coton. Unsteady strong shock interactions in a transonic turbine: experimental and numerical analysis. *Journal of Propulsion and Power*, 24(4):722–731, 2008.
- D. Papadogiannis, F. Duchaine, L. Gicquel, G. Wang, and S. Moreau. Effects of Subgrid Scale Modeling on the Deterministic and Stochastic Turbulent Energetic Distribution in Large-Eddy Simulations of a High-Pressure Turbine Stage. *Journal of Turbomachinery*, 138(9), 04 2016. ISSN 0889-504X. doi: 10.1115/1.4032844. URL <https://doi.org/10.1115/1.4032844>. 091005.
- L. Pinelli, M. Marconcini, R. Pacciani, P. Gaetani, and G. Persico. Computational and Experimental Study of the Unsteady Convection of Entropy Waves Within a High-Pressure Turbine Stage. *Journal of Turbomachinery*, 143(9), 05 2021. ISSN 0889-504X. doi: 10.1115/1.4050600. URL <https://doi.org/10.1115/1.4050600>. 091011.
- P.L. Roe. Approximate Riemann solver, parameter vector and differences schemes. *Journal of Computational Physics*, 43:357–372, 1981.
- R. D. Sandberg and V. Michelassi. Fluid dynamics of axial turbomachinery: Blade- and stage-level simulations and models. *Annual Review of Fluid Mechanics*, 54(1):255–285, 2022. doi: 10.1146/annurev-fluid-031221-105530. URL <https://doi.org/10.1146/annurev-fluid-031221-105530>.
- C. Sieverding and M. Manna. A review on turbine trailing edge flow. *International Journal of Turbomachinery, Propulsion and Power*, 5(2), 2020. ISSN 2504-186X. doi: 10.3390/ijtp5020010. URL <https://www.mdpi.com/2504-186X/5/2/10>.
- M. Soismier. *Stratégie de résolution hybride structurée / non structurée pour la simulation d'effets technologiques en turbomachines*. Theses, Université Grenoble Alpes, October 2016. URL <https://theses.hal.science/tel-02628491>.
- J. A. Tallman, C. W. Haldeman, M. G. Dunn, A. K. Tolpadi, and R. F. Bergholz. Heat Transfer Measurements and Predictions for a Modern, High-Pressure, Transonic Turbine, Including Endwalls. *Journal of Turbomachinery*, 131(2), 01 2009. ISSN 0889-504X. doi: 10.1115/1.2985072. URL <https://doi.org/10.1115/1.2985072>. 021001.
- G. D. van Albada, B. van Leer, and W. W. Roberts. *A Comparative Study of Computational Methods in Cosmic Gas Dynamics*, pages 95–103. Springer Berlin Heidelberg, Berlin, Heidelberg, 1997. ISBN 978-3-642-60543-7. doi: 10.1007/978-3-642-60543-7\_6. URL [https://doi.org/10.1007/978-3-642-60543-7\\_6](https://doi.org/10.1007/978-3-642-60543-7_6).
- V. Venkatakrishnan. Convergence to steady state solutions of the euler equations on unstructured grids with limiters. *Journal of Computational Physics*, 118(1):120–130, 1995. ISSN 0021-9991. doi: <https://doi.org/10.1006/jcph.1995.1084>. URL <https://www.sciencedirect.com/science/article/pii/S0021999185710844>.
- T. Yasa, G. Paniagua, and R. Dénos. Application of Hot-Wire Anemometry in a Blow-Down Turbine Facility. *Journal of Engineering for Gas Turbines and Power*, 129(2):420–427, 02 2006. ISSN 0742-4795. doi: 10.1115/1.2364191. URL <https://doi.org/10.1115/1.2364191>.
- S. Yoon and D. Kwak. Three-dimensional incompressible navier-stokes solver using lower-upper symmetric-gauss-seidel algorithm. *AIAA Journal*, 29(6):874–875, 1991. doi: 10.2514/3.10671. URL <https://doi.org/10.2514/3.10671>.